JOURNAL OF MATERIALS SCIENCE 39 (2004) 861–865

Fabrication of textured alumina by electrophoretic deposition in a strong magnetic field

T. UCHIKOSHI, T. S. SUZUKI, H. OKUYAMA, Y. SAKKA
Materials Engineering Laboratory, National Institute for Materials Science (NIMS), 1-2-1 Sengen, Tsukuba, Ibaraki 305-0047, Japan
E-mail: Uchikoshi.Tetsuo@nims.go.jp

Textured alumina ceramics were fabricated by electrophoretic deposition in a strong magnetic field of 10 T (Tesla) followed by sintering. Single crystalline α-alumina particles dispersed in aqueous media were aligned due to their anisotropic diamagnetic susceptibility and then deposited on a cathodic substrate. The degree of crystalline orientation of the as-deposited specimen characterized by X-ray diffraction was small but highly improved by sintering in the temperature range of 1273–1873 K. Microstructural observations showed the absence of any anisotropic grain growth.

1. Introduction

There has been increased interest in textured ceramics since they have anisotropic mechanical, thermal and electrical properties, which have values similar to single crystals [1]. Textured ceramics have been produced by a variety of techniques, such as tape casting [2], hot forging or deformation [3–5], eutectic solidification [6], templated or seeded grain growth [7–9]. Ceramic platelets, fibers or whiskers are used as seed particles along with some additives to promote the anisotropic grain growth during sintering [9]. Although it is important to make a distinction between the microstructural texture and crystalline texture [10], they have often been confused.

Recently, we have reported that crystalline-textured ceramics could be obtained by slip casting in a strong magnetic field using magnetic anisotropy that originates from the crystal structures [11, 12]. Many materials in non-cubic crystal structures have anisotropic magnetic susceptibilities, $\Delta\chi = \chi_{//}\text{-}\chi_{\perp}$, associated with their crystal structures, where $\chi_{//}$ and $\chi_{\perp}$ are the susceptibilities parallel and perpendicular to the magnetic principal axis, respectively. The energy of anisotropy is given as [13]:

$$\Delta E = \Delta\chi V B^2/2\mu_0, \quad (1)$$

where V is the volume of the material, B is the applied magnetic field, and μ_0 is the permeability in a vacuum. The energy of anisotropy is the driving force for magnetic alignment, however, the energy of nonferromagnetic materials is usually small and its influence has not been taken into consideration so far. The recent development of superconducting magnet technologies has enabled one to introduce magnetic fields as high as 10 T in academic laboratories. Under such strong magnetic fields, the magnetization force acting on feeble magnetic materials such as alumina is not negligible. α-alumina (corundum) has a small anisotropic diamagnetic susceptibility of $\Delta\chi = 4.19 \times 10^{-9}$ emu [14, 15]. The energies of anisotropy estimated from Equation 1 for a spherical, single-crystalline α-alumina particle are 8.78×10^{-23} J in a 1 T magnetic field and 8.78×10^{-21} J in 10 T, assuming that the particle size is 0.2 μm. On the other hand, the energy of thermal motion kT at 300 K is 4.14×10^{-21} J, where k is Boltzmann's constant. These values suggest that the energy of anisotropy in a strong magnetic field can be higher than the energy of thermal motion at room temperature ($\sim kT$). Diamagnetic materials with a magnetic anisotropy have the potential ability to align in a strong magnetic field. It is essential for each particle to be single crystalline and not to be flocculated [16].

In the present study, crystalline-textured alumina was fabricated by electrophoretic deposition (EPD) [17–19] in a strong magnetic field using a deflocculated suspension of single crystalline alumina particles.

2. Experimental procedures

Nearly spherical, single crystalline α-alumina particles (Sumitomo Chem. Co., Ltd., AKP-50, average particle size of 0.2 μm, high purity of >99.99%) were dispersed at pH 4 in distilled water by ultrasound, and then a deflocculated aqueous suspension with a 10 vol% solid content was prepared. The suspension was placed in a superconducting magnet (Japan Magnet Technology JMTD-10T100 with a bore of 100 mm) and then a strong 10 T magnetic field was applied to the suspension to rotate the particles. A pair of electrodes, with an area of 20×20 mm^2 and 20 mm spacing, held on a phenol resin support was put in the suspension and then an electrical current was applied. The magnetic field was maintained on the suspension during the EPD

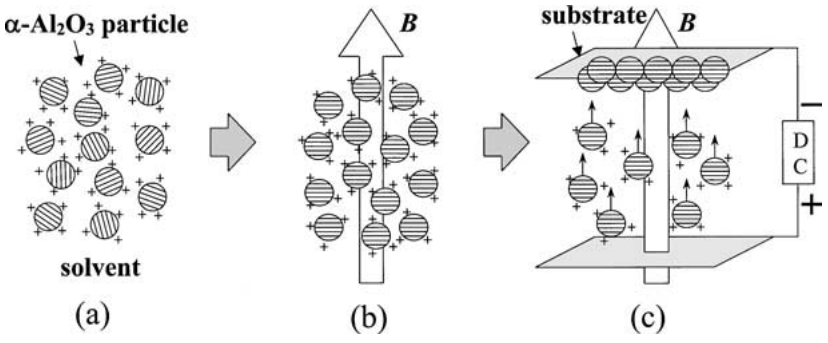

Figure 1 Schematic diagram of the concept and the experimental setup of the electrophoretic deposition in a strong magnetic field: (a) deflocculated alumina suspension, (b) alignment of the particles in a strong magnetic field and (c) electrophoretic deposition in the magnetic field.

at a constant voltage of 30 V at room temperature. The direction of the magnetic field parallel to that of the particle's flow was not affected by the Lorentz force. A palladium sheet was used as the cathodic substrate to absorb hydrogen produced by electrolysis of the solvent [20]; therefore, bubble-free and dense deposits were produced. A schematic illustration of the experimental procedure is shown in Fig. 1. The green compacts were presintered at 1073 K for 2 h so as to cut them at the planes which are parallel and perpendicular to the magnetic field. The sintering was conducted at fixed temperatures between 1273–1873 K for 2 h in air and not in the magnetic field. The density of the sintered compacts was measured by Archimedes' method using kerosene. X-ray diffraction (XRD) analysis and microstructural observations were carried out for the cross-sectional planes which were parallel and perpendicular to the magnetic field. Hereafter, these planes are designated PL- and PR-planes, respectively.

3. Results and discussion

Fig. 2 shows the densification behavior of the samples as a function of sintering temperature. Samples presintered at 1073 K exhibited similar densities as those of the green compacts (∼59% TD) and no difference was observed between the samples deposited in and out of the magnetic fields. Densification occurs above 1073 K and the densities reach ∼97% TD at 1873 K.

Fig. 3 shows the XRD patterns of the α-alumina deposited at 10 T, followed by presintering at 1073 K for 2 h. Slight differences in the XRD peaks between the PL- and PR-planes show some crystalline orientation.

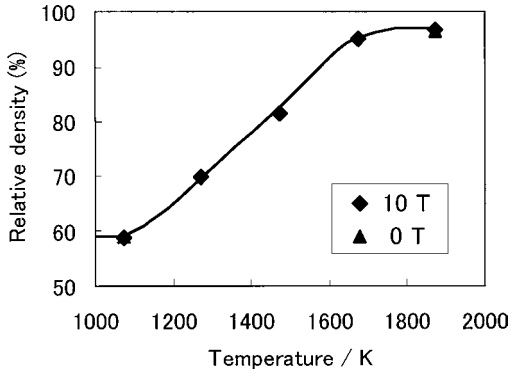

Figure 2 Change in the relative density of the samples as a function of sintering temperature.

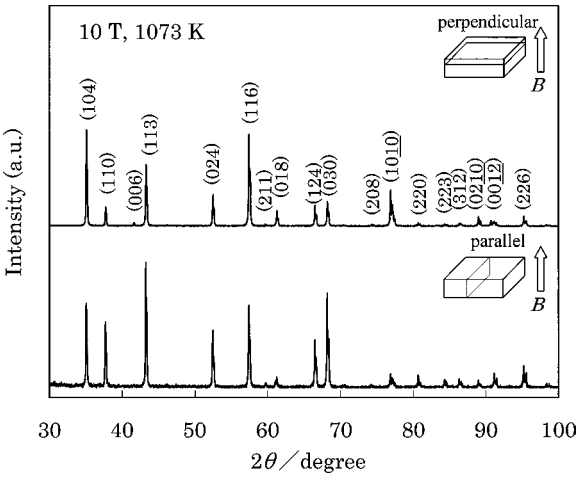

Figure 3 X-ray diffraction patterns of the α-alumina deposited at 10 T followed by presintering at 1073 K.

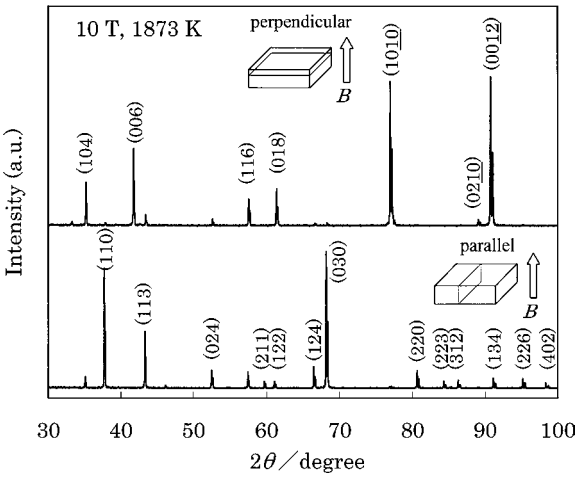

Figure 4 X-ray diffraction patterns of the α-alumina deposited at 10 T followed by sintering at 1873 K.

The differences in the peaks are obvious after the sintering at 1873 K as shown in Fig. 4. To characterize the XRD peaks, the interplanar angles ϕ_{hkl} between the planes (hkl) and the basal plane $(00L)$ are calculated for a hexagonal unit cell of α-alumina ($a = 0.4758$ nm, $c = 1.2991$ nm) [19] using Equation 2 [22] and are listed in Table I.

$$\cos\phi_{\mathrm{hkl}} = \frac{\frac{\sqrt{3}a}{2c}l}{\sqrt{h^2 + k^2 + hk + \frac{3a^2}{4c^2}l^2}} \qquad (2)$$

TABLE I XRD data of α-alumina, corundum (ICDD 10–173) and the interplanar angles ϕ_{hkl} between the planes (hkl) and the basal plane ($00L$) calculated for a hexagonal unit cell of α-alumina

d(Å)	2θ(Cu k$_\alpha$) (deg)	I/I_o	hkl	ϕ (deg)
3.479	25.582	75	012	57.61
2.552	35.134	90	104	38.25
2.379	37.782	40	110	90
2.165	41.682	1	006	0
2.085	43.36	100	113	61.22
1.964	46.181	2	202	72.4
1.74	52.549	45	024	57.61
1.601	57.515	80	116	42.31
1.546	59.765	4	211	83.16
1.514	61.161	6	122	76.52
1.51	61.341	8	018	21.51
1.404	66.543	30	124	64.38
1.374	68.193	50	030	90
1.337	70.354	2	125	59.06
1.276	74.263	4	208	38.25
1.239	76.876	16	1010	17.5
1.2343	77.223	8	119	31.25
1.1898	80.688	8	220	90
1.16	83.212	1	306	57.61
1.147	84.371	6	223	74.64
1.1382	85.177	2	311	84.97
1.1255	86.371	6	312	80.02
1.1246	86.457	4	128	46.2
1.0988	89.013	8	0210	32.23
1.0831	90.657	4	0012	0
1.0781	91.196	8	134	70.61
1.0426	95.255	14	226	61.22
1.0175	98.401	2	402	80.99

The diffraction peaks of the planes at low interplanar angles such as (006)($\phi_{006} = 0°$), (00$\underline{12}$)($\phi_{00\underline{12}} = 0°$) and (10$\underline{10}$)($\phi_{10\underline{10}} = 17.5°$) are characteristic of the PR-plane. In contrast, the diffraction peaks of the planes at high interplanar angles such as (110)($\phi_{110} = 90°$), (030)($\phi_{030} = 90°$), (220)($\phi_{220} = 90°$), (211)($\phi_{211} = 83.16°$) and (312)($\phi_{312} = 80.02°$) are characteristic of the PL-plane. The XRD data clearly show the crystallite orientation of the α-alumina prepared in the strong magnetic field of 10 T. It is also shown that the c-axis is easily aligned along the magnetic field.

Fig. 5 shows the XRD patterns of the α-alumina deposited at 0 T (external to the magnetic field) followed by sintering at 1873 K for 2 h. No difference is observed between the XRD patterns of the PL- and PR-planes. It is obvious that the specimen prepared with no magnetic field has a randomly oriented polycrystalline structure.

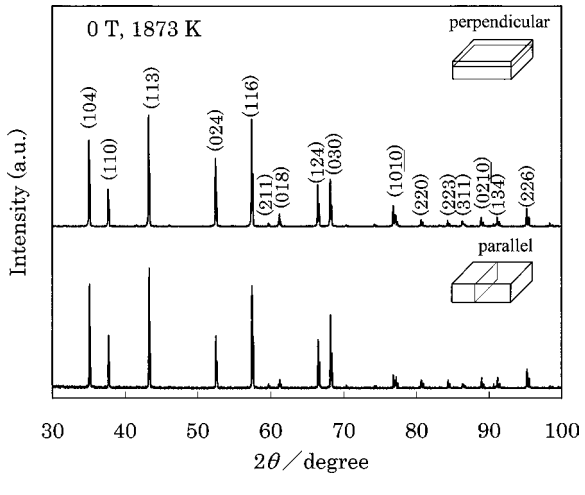

Figure 5 X-ray diffraction patterns of the α-alumina deposited at 0 T (external to the magnetic field) followed by sintering at 1873 K.

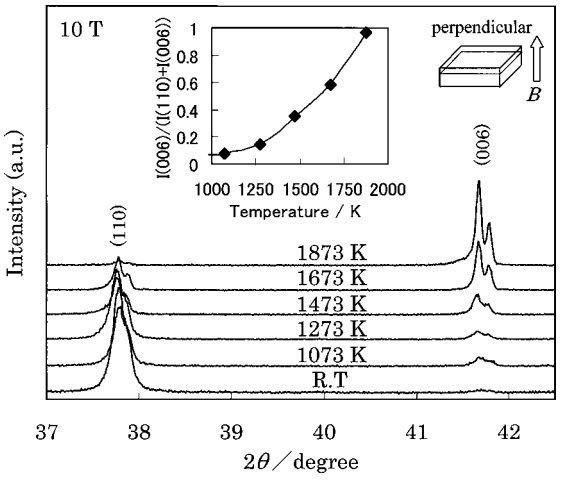

Figure 6 Changes in the diffraction peaks of the (110)($\phi_{110} = 90°$) and (006)($\phi_{006} = 0°$) planes of the PR-plane with sintering temperatures.

Fig. 6 shows the changes in the diffraction peaks of the planes (110)($\phi_{110} = 90°$) and (006)($\phi_{006} = 0°$) of the PR-plane versus the sintering temperature. The change of the intensity ratios $I_{006}/(I_{110} + I_{006})$ is also shown in this figure. The peak of (006), which should be extremely weak for randomly oriented alumina, becomes stronger with increasing temperature. In contrast, the peak of (110), which should be strong, becomes weaker with temperature. Fig. 6 also shows that the degree of orientation is improved during sintering. The average orientation angle $\bar{\phi}$ of the crystallites was estimated from all the diffraction peaks of the PL- and PR-planes in the 2θ range of 25°–100° using Equation 3 [23].

$$\bar{\phi} = \frac{1}{2}\left[\underbrace{\frac{\sum(I_{hkl} \times \phi_{hkl})}{\sum I_{hkl}}}_{\text{PR-plane}} + \underbrace{\frac{\sum(I_{hkl} \times (90 - \phi_{hkl}))}{\sum I_{hkl}}}_{\text{PL-plane}}\right] \tag{3}$$

where ϕ_{hkl} is the interplanar angle listed in Table I. Fig. 7 shows the average orientation angle $\bar{\phi}$ of the crystallites as a function of sintering temperature. The average orientation angle of the sample deposited at 10 T followed by sintering at 1027 K is 39.0°. A slight orientation is observed for the sample deposited at 10 T, however, the degree of orientation is not very high up to 1273 K. On the other hand, densification occurs above 1073 K as shown in Fig. 2. This difference in the temperature shows that the densification steps and orientation improvement are not the same ones. It is generally known that the improvement in orientation is accompanied by grain growth. If adjacent grains have a similar orientation, grain growth will be enhanced because of the low grain boundary energy. Less-oriented small grains (the energy of rotation ΔE in Equation 1 is proportional to the volume of a particle) will merge into well-oriented

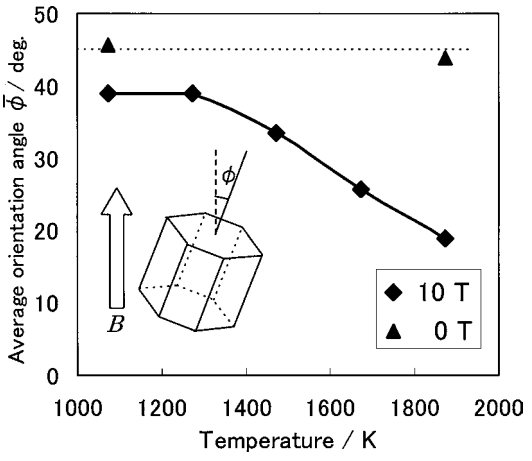

Figure 7 Average orientation angle $\bar{\phi}$ of the crystallites as a function of sintering temperature.

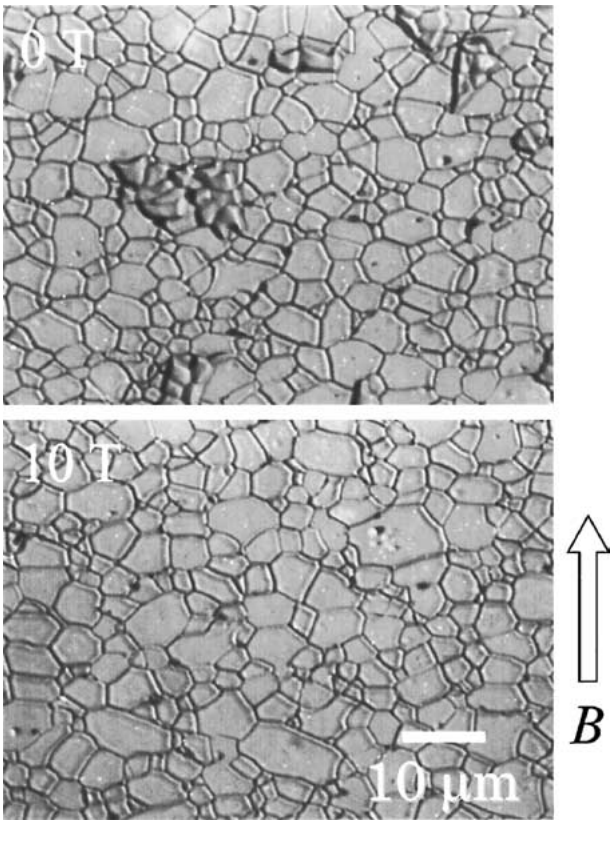

Figure 8 Microstructures of the PL-planes observed for the samples sintered at 1873 K. Deposition was carried out at 0 T or 10 T.

large grains during grain growth. Above 1273 K, the orientation angle $\bar{\phi}$ decreases with temperature and it reaches 18.8° at 1873 K. The angle $\bar{\phi}$ measured for the samples prepared at 0 T is close to 45° and it represents a random orientation for the alumina consolidated at 0 T.

Fig. 8 shows the microstructures of the PL-planes observed for the samples sintered at 1873 K. Thermal etching of the polished surfaces was conducted at 1773 K for 2 h. No obvious difference was observed between the samples deposited at 0 T and 10 T. One of the characteristics of this textured alumina is that it is not accompanied by anisotropic grain growth and has equiaxed grains. It has been demonstrated that the electrophoretic deposition in a strong magnetic field is an excellent method to obtain a strong crystalline texture in the absence of a microstructural texture.

4. Conclusions

Positively charged, single crystalline α-alumina particles in the aqueous suspension of 10 vol% solid were deposited on the palladium substrates by the electrophoretic deposition in a strong magnetic field of 10 T. The degree of crystalline orientation of the as-deposited specimen characterized by XRD analysis was small but highly improved by the following sintering. The average crystalline orientation angle of the alumina sintered at 1873 K was estimated to be 18.8° from the XRD peaks. Although strong crystalline texture was confirmed by XRD analysis, no microstructural texture was observed. No obvious differences of the green and sintered densities were found between the samples deposited in and out of the magnetic fields. It was demonstrated that the EPD in a strong magnetic field is a promising processing technique for making crystalline textured ceramics.

Acknowledgment

The authors wish to thank Dr. Fenqiu Tang at NIMS for her help with the EPD experiments, Prof. Patrick S. Nicholson at McMaster University and Dr. Partho Sarkar at the Alberta Research Council for their valuable comments.

References

1. E. SUVACI and G. L. MESSING, *J. Amer. Ceram. Soc.* **83** (2000) 2041.
2. K. HIRAO, M. OHASHI, M. E. BRITO and S. KANZAKI, *ibid.* **78** (1995) 1687.
3. T. TAKENAKS and K. SAKATA, *Jpn. J. Appl. Phys.* **19** (1980) 31.
4. Y. MA and K. J. BOWMAN, *J. Amer. Ceram. Soc.* **74** (1991) 2941.
5. Y. YOSHIZAWA, M. TORIYAMA and S. KANZAKI, *ibid.* **84** (2001) 1392.
6. V. S. STUBICAN and R. C. BRADT, *Annu. Rev. Mater. Sci.* **11** (1981) 267.
7. S. H. HONG and G. L. MESSING, *J. Amer. Ceram. Soc.* **82** (1999) 867.
8. E. SUVACI, K.-S. OH and G. L. MESSING, *Acta Mater.* **49** (2001) 2075.
9. M. M. SEABAUGH, I. H. KERSCHT and G. L. MESSING, *J. Amer. Ceram. Soc.* **80** (1997) 1181.
10. D. BRANDON, D. CHEN and H. CHAN, *Mater. Sci. Eng.* A **195** (1995) 189.
11. T. S. SUZUKI, Y. SAKKA and K. KITAZAWA, *Adv. Eng. Mater.* **3** (2001) 490.
12. T. S. SUZUKI and Y. SAKKA, *Jpn. J. Appl. Phys.* **44** (2002) L1272.
13. P. DE RANGO, M. LESS, P. LEJAY, A. SULPICE, R. TOURNIER, M. INGOLD, P. GERMI and M. PERNET, *Nature* **349** (1991) 770.
14. C. UYEDA, *Phy. Chem. Miner.* **20** (1993) 77.
15. *Idem., Jpn. J. Appl. Phys.* **32** (1993) L298.
16. T. UCHIKOSHI, T. S. SUZUKI, H. OKUYAMA and Y. SAKKA, *J. Mater. Res.* **18** (2003) 254.
17. P. SARKAR and P. S. NICHOLSON, *J. Amer. Ceram. Soc.* **79** (1996) 1987.

18. I. ZHITOMIRSKY, *Adv. Coll. Interf. Sci.* **97** (2002) 279.
19. A. R. BOCCACCINI and I. ZHITOMIRSKY, *Curr. Opin. Solid State Mater. Sci.* **6** (2002) 251.
20. T. UCHIKOSHI, K. OZAWA, B. D. HATTON and Y. SAKKA, *J. Mater. Res.* **16** (2001) 321.
21. ICDD (JCPDS) #10-173 [corundum].
22. B. D. CULLITY, "Elements of X-ray Diffraction" (Addison Wesley Pub. Co. Inc., London, 1959) p. 460.
23. T. TAHASHI, M. ISHIHARA, K. SASSA and S. ASAI, *Mater. Trans.* **44** (2003) 285.

Received 16 January
and accepted 30 June 2003